Flow Measurement and Instrumentation ∎ (∎∎∎∎) ∎∎∎–∎∎∎

Contents lists available at ScienceDirect

Flow Measurement and Instrumentation

journal homepage: www.elsevier.com/locate/flowmeasinst

Imaging of gas–liquid annular flows for underbalanced drilling using electrical resistance tomography

Wei Na [a,*], Jiabin Jia [b,1], Xin Yu [a], Yousef Faraj [b], Qiang Wang [b], Ying-feng Meng [a], Mi Wang [b], Wantong Sun [a]

[a] Sate Key Laboratory of O&G Reservoir Geology and Exploitation, Southwest Petroleum University, China
[b] School of Process and Chemical Engineering, University of Leeds, LS2 9JT, UK

ARTICLE INFO

Article history:
Received 10 November 2014
Received in revised form
23 June 2015
Accepted 18 July 2015

Keywords:
Underbalanced drilling technique
Annular flow
Flow regime
Electrical resistance tomography
Flow regime visualisation

ABSTRACT

The underbalanced drilling technique, which is also known as managed-pressure drilling, is playing an important role in oil and gas sector, as it reduces common conventional drilling problems such as minimal drilling rates and formation damage, differential sticking and lost circulation. Flow regime monitoring is one of the key topics in annular multiphase flow research, particularly for underbalanced drilling technique. Prediction of the prevailing flow regime in an annulus is of particular importance in the design and installation of underbalanced drilling facilities. Especially, for establishing a suitable pressure-drop model based on the characteristics of the active flow regime. The methods of flow regime prediction (or visualisation) in an annulus that are currently in use are very limited, this is evidently due to poor accuracy or they are simply not applicable to underbalanced drilling operation in practice. Therefore, this paper presents a monitoring method, in which Electrical Resistance Tomography (ERT) is used to rapidly image the prevailing flow regime in an annulus with a metallic inner pipe. Experiments were carried out using an air–water flow loop with a test section 50 mm diameter flow pipe. The two-phase air–water flow regimes are visualised in the upward vertical annulus with a radius ratio (r/R) 0.4. This paper highlights the visualisation results of only three flow regimes, namely bubble flow, transitional bubble-slug flow and slug flow. The flow regimes are visualised through axial images stacked from 50 mm diameter-pixels of 2D tomograms reconstructed with the Conjugate Gradient Method (SCG). Gas volume fraction profiles within the annular flow channel are also illustrated. The profiles are extracted using the Modified Sensitivity coefficient Back-Projection (MSBP) method with a sensitivity matrix generated from a realstic phantom in the finite element method software. The results are compared with visual observations (e.g. photographs) of the active flow regime at the time of ERT measurements.

1. Introduction

The growing number of reservoirs around the world and the need for recovering hydrocarbons more efficiently and effectively has been the driving force for oil and gas industry to continuously improve the drilling process. A variety of drilling techniques have been investigated and many of them are currently used in oil and gas industry. One of such techniques is called Underbalanced drilling (UBD), which allows drilling a well more economically, efficiently and safely [15]. The UBD is the process, in which the wellbore pressure is deliberately designed to be lower than the process of the formation that is drilled. The underbalanced pressure conditions facilitate the reservoir fluids to enter the wellbore during drilling, thus preventing fluid loss and related causes to formation damage [2]. In order to achieve UBD conditions, a simultaneous injection of a mixture of two-phase liquid and gas is required. The two-phase mixture is directly injected into the drill string at the surface, and then the returning fluid is flowing back in an upward vertical fashion in the annulus, outside the drill string [18]. The liquid–gas mixture flows in the annulus according to several topological configurations, which are called flow regimes, these are namely bubble flow, slug flow, churn flow and annular flow [7]. Prediction and monitoring these flow regimes are of particular importance for optimisation, diagnostics and control of the process, especially for establishing a suitable pressure drop model in an annulus. As reported in literature that an accurate

* Corresponding author.
E-mail addresses: weina8081@163.com (W. Na), m.wang@leeds.ac.uk (M. Wang).
[1] Current address: Institute For Digital Communication, School of Engineering, University of Edinburgh, EH9 3JL, Edinburgh.

http://dx.doi.org/10.1016/j.flowmeasinst.2015.07.003

annular multiphase flow pressure drop model for underbalanced drilling is highly required [12]. As in UBD process the control of pressure in the wellbore is very important [14]. The visualisation of these flow regimes in the annulus can provide valuable information and whereby conduct a safe and effective drilling [3].

The study of two-phase flow in an annulus has received a significant attention from previous researchers; this is clearly due to its practical application. Some of these studies have focused on theoretical predictions of flow regimes within the annulus, however, due to the complex nature of flow phenomena, the prediction of flow behaviour and monitoring the flow regimes are quite difficult to make, through theoretical approach. In addition, most of the existing steady-state multiphase flow experimental investigations are based on low viscous Newtonian fluids, while the fluids and its physicochemical properties in the condition of the down-hole are very different. Therefore, the calculation of multiphase flows with the existing multiphase flow theories deviates from the actual values [8].

Over the years, the researchers have managed to develop some flow regime transition models for annular geometry. However, the prediction accuracy of these models is questionable when they are checked with additional experimental data, particularly when the flow regime is slug or churn. Moreover, a wide range of measurement techniques have been reported, so as to provide phase distribution information within an annulus, hence facilitating the design of the processes and visualisation of flow structure, particularly in drilling wells. [13] used conductivity probes for direct analysis of flow behaviour in vertical annular flow. Their visualisation method is quite straightforward, however, it is associated with a major limitation that it does not provide visual observation of the whole pipe cross section; in addition the transparency of the pipe wall is also a major issue. Therefore, in order to provide a clear structure of flow and visualise phase distribution within an opaque annulus, an Electrical Resistance Tomography is a promising technique to non-invasively and rapidly image the internal structure of an annular flow. Recently, a non-linear ERT reconstruction algorithm has been proposed for reconstructing phase distribution within an annulus [17]. They concluded that using ERT, with their developed algorithm, can provide a valuable tool to interrogate the internal structure of an annular flow.

ERT is an imaging technique that can capture the internal structure of a two-phase flow within an opaque pipe or vessel [21,23,24]. The principle of ERT is based on the difference in the conductivity of the constituent phases within multiphase flow domain. It has been successfully applied on many industrial processes, such as mixing, multiphase flow and so on. The basic principle of ERT operation is that the flow process is interrogated by an array of electrodes (typically 16 electrodes) at the periphery of the pipe wall. An electrical current is injected through a pair of electrodes and the voltage is measured through the remaining electrodes. The main advantage of ERT is that non-intrusive, relatively inexpensive, fast and safe. Therefore, it can provide a unique opportunity to visualise the internal structure of a two-phase flow in an annulus.

A good agreement between results from ERT and a mesh sensor for air volume fraction measurement of air-water upward flows was reported in our previous work [4]. This study mainly presents an online visualisation technique, in which ERT is utilised to rapidly image the internal structure of co-current gas–liquid vertical flow. A corrected sensitivity map and the conjugate gradient method (SCG) [20] with an annular finite element mesh is used, to offer an effective way of visualising multiphase flow in an opaque annulus with high pressure and providing a 2- or 3-D spatial and temporal distribution of each constituent phase. In addition, gas volume fraction profiles in an annulus are also measured using Modified Sensitivity coefficient Back-Projection (MSBP) method. The results are compared with visual observations of the flow within the annulus (e.g. photographs).

2. Imaging theory

2.1 Sensitivity matrix

The adjacent sensing strategy [1] is commonly used for the industrial ERT. In this sensing strategy, one of two adjacent electrode pairs is initially connected with the electric source and the voltages are sensed from the remaining adjacent electrode pairs. The procedure is sequentially repeated by switching the electric source to next electrode pairs (ref). The voltage change measured on one pair of electrodes is approximately linearized as product between the sensitivity matrix **S** and the conductivity change *on one or more areas* within the sensing domain, as the conductivity change is much smaller than the base conductivity (Eq. (1)) . The image reconstruction is the process of inversely computing the conductivity change vector $\mathbf{\Delta\sigma}$ with known boundary voltage vector $\mathbf{\Delta V}$ and sensitivity matrix **S.** The elementary description of vector multiplication for the jth voltage change is given as,

$$\Delta V_j = \sum_{k=1}^{K} s_{j,k} \cdot \Delta\sigma_k \tag{1}$$

where $j=1, 2, \cdots, J$ and $k=1, 2, \cdots, K$; J and K denote the maximum number of independent voltage measurements on boundary electrode pairs (104 in the case of 16 electrodes per ERT sensor) and the total number of pixels on the 2-dimensional imaging domain a_k, respectively.

At a pixel k of sensing domain with a homogenous base conductivity, the elementary jth sensitivity coefficient of the sensitivity matrix for a current-driven electrode pair m and a voltage measurement electrode pair n is given by Eq. (2) below.

$$s_{j,k} = -\int_{a_k} \frac{\nabla\Phi_m}{I_m} \cdot \frac{\nabla\Psi_n}{I_n} da_k \tag{2}$$

where $\nabla\Phi_m$ and $\nabla\Psi_m$ are potential gradients over pixel a_k due to current-driven electrode pair m and n respectively. The integration is made over the area of pixel k. The sensitivity matrix **S** is a $j \times k$ matrix, which is composed from the sensitivity coefficient over the whole sensing domain A.

The recent research work found that based on the nonlinear approximation, the modified sensitivity back-projection (MSBP) method as expressed in Eq. (3) [19,20] is a more accurate approximation than the traditional linear back-projection method [9] to obtain the kth conductivity ratio σ_k/σ_1 [6].

$$\frac{\sigma_k}{\sigma_1} \approx \frac{\sum_{j=1}^{J} s_{k,j}}{\sum_{j=1}^{J} s_{k,j} \cdot \frac{V_j'}{V_j}} \tag{3}$$

where $s_{k,j}$ is an element of the transpose matrix of the sensitivity matrix **S**, V_j is the jth baseline voltage measured on ERT sensor containing only single continuous phase with conductivity σ_1, and $V_j'$is the jth voltage measured on ERT sensor after two phase mixture presents and conductivity is altered to σ_k.

The Finite Element Method (FEM) software like COMSOL can simulate this process and compute the sensitivity map. Fig. 1 graphically shows the sensitivity map of a conventional circular ERT sensor with adjacent sensing strategy. The 3D view of Fig. 1 (b) demonstrates that in the circular sensing domain, the peripheral area is more sensitive to the conductivity change than the central area.

In this work, the annular flow of unbalanced drilling is studied

Please cite this article as: W. Na, et al., Imaging of gas–liquid annular flows for underbalanced drilling using electrical resistance tomography, Flow Measurement and Instrumentation (2015), http://dx.doi.org/10.1016/j.flowmeasinst.2015.07.003

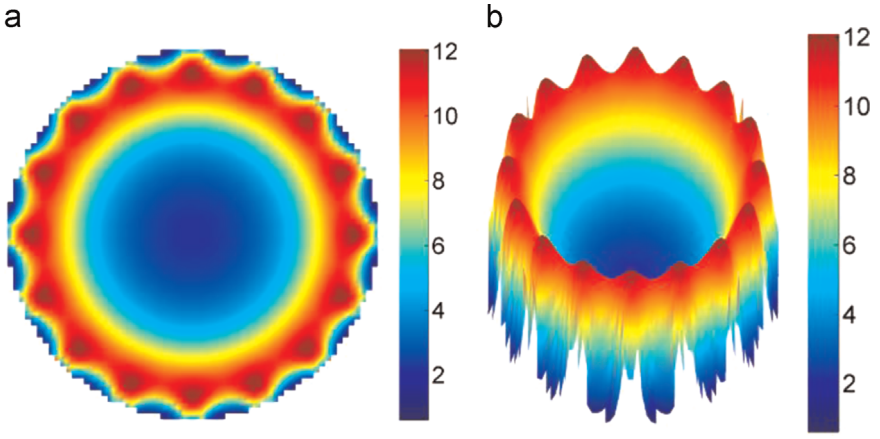

Fig. 1. Conventional sensitivity map. (a) Top view and (b) 3D view.

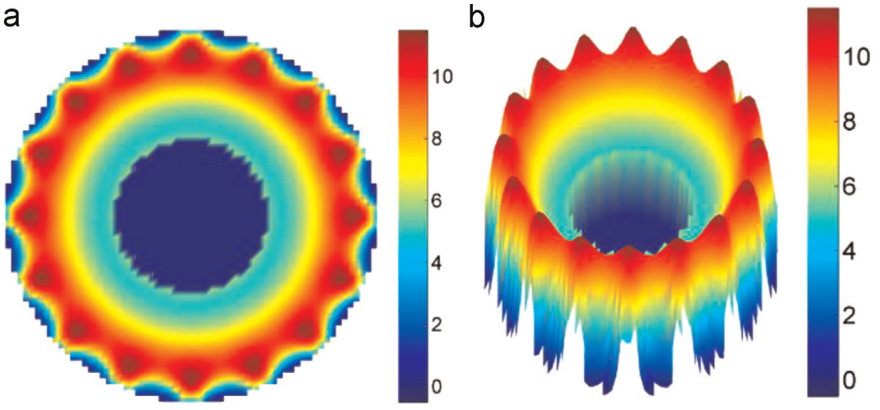

Fig. 2. Unique sensitivity map. (a) Top view and (b) 3D view.

using ERT imaging technique. In the experiment, the diameter of the flow pipe is 50 mm. A steel pipe with 20 mm diameter is inserted at the centre of the pipe. Rather than using conventional sensitivity matrix of Fig. 1, a realistic phantom in the FEM software should be built to compute the unique sensitivity matrix for ERT image reconstruction. Since the metallic pipe provides an equipotential to the inner wall of the annulus, as shown in Fig. 2, electrical field (V/m) abruptly drops to zero within the region of the solid steel pipe, which will lead to constant grey column on reconstructed ERT images as given in Section 4.

A new mesh file was generated with corresponding boundary conditions for a 192 elements and 141 nodes finite element mesh as shown in Fig. 3(a). Typical images reconstructed with SCG method are illustrated by Fig. 3(b) and (c) in correspondence to flow conditions of bubble flow (Vsa = 0.085 m/s, Vsw = 1.039 m/s) and slug flow (Vsa = 0.425 m/s, Vsw = 0.342 m/s).

2.2 Correlation between conductivity and volume fraction

ERT produces not only images with respect to conductivity distribution, but the local and overall volume fraction of dispersed phase in the two-phase flow. The Maxwell relationship [11] formulated in Eq. (4) with the zero conductivity of particles is mostly used to correlate the kth local gas volume fraction c_k over pixel a_k

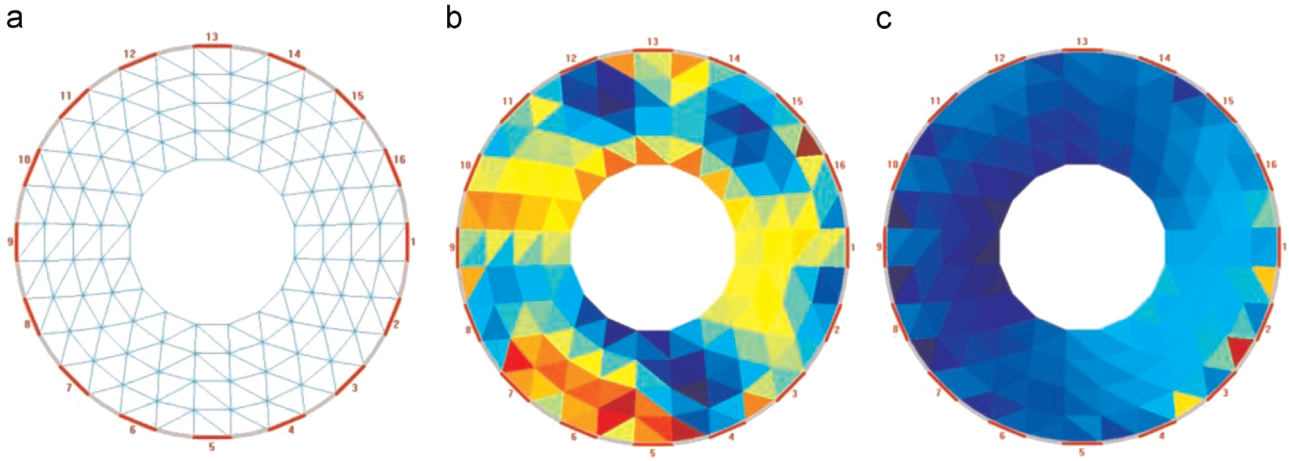

Fig. 3. Annular mesh (a), cross section images of bubble flow (b) and slug flow (c).

Please cite this article as: W. Na, et al., Imaging of gas–liquid annular flows for underbalanced drilling using electrical resistance tomography, Flow Measurement and Instrumentation (2015), http://dx.doi.org/10.1016/j.flowmeasinst.2015.07.003

in gas–liquid flow from the corresponding local conductivity σ_k with the assumption of gas volumetric distribution in an element to be homogeneous. In addition, the applicability of Maxwell relationship to high volume fraction were reported [5,16,6]

$$c_k = \frac{2\sigma_1 - 2\sigma_k}{\sigma_k + 2\sigma_1} = \frac{2 - 2\frac{\sigma_k}{\sigma_1}}{2 + \frac{\sigma_k}{\sigma_1}} \tag{4}$$

where σ_1 is the conductivity of background continuous phase (water), σ_k is the local gas–liquid mixture conductivity derived from ERT and $k=1,2,\ldots,K$.

3. Experimental set-up

A set of tests were carried out using the non-pressurised multiphase flow facility at the University of Leeds. A schematic diagram of the flow facility is illustrated in Fig. 4. The pipeline is of Plexiglas with 50 mm internal diameter and 5 mm wall thickness. Air and tap water was used at room temperature. The flow loop facilitates separate injection of water and air at the horizontal section and eventually mixed up after the loop bend, where the mixture of water and air is introduced to the vertical upward flow test section. The injection of air and water into the flow loop is highlighted by different coloured lines in Fig. 4. The water injection stream is presented by a blue line; air injection stream is presented by a red line, while the green line denotes the mixture of air and water flow. The loop is an open recirculating flow loop. This means that after injecting air and water, the mixture goes through the vertical test section and returned to a holding tank through a horizontal returning limb (5.8 m length). The air is released into the atmosphere at the discharge point, while water is returned into the tank and reintroduced into the flow loop. The recycled water is reintroduced into the loop through a jet pump, which connects the downstream of the loop to the water tank. The inlet water flow rate is controlled through a ball valve and measured using a water turbine flow meter (Omega). The inlet air flow rate is controlled through a gas mass flow controller (Omega FMA5542, 0-100 Standard Litre per Minute (SLPM)).

The test section is located within the 3 m long vertical section, on which a dual-plane ERT sensor, an Electromagnetic Flow meter (EMF), two absolute pressure transducers, a temperature sensor and an annular section are installed. The dual-plane ERT sensor located upstream the EMF, as shown in Fig. 4. At the periphery of each sensor plane, 16 equally spaced stainless steel electrodes are mounted. The upstream sensor plane is separated from the downstream sensor plane by 50 mm. The annulus section consists of a metallic inner pipe (OD=20 mm), which is suspended inside the outer pipe (ID=50 mm). Thus the radius ratio of the annulus (r/R) is 0.4. The annulus test section is confined within a sealed cubical water filled observation section to avoid refraction on the circular pipe wall during visual observations (photograph), as illustrated in Fig. 5. The lighting was also provided to facilitate the observation of flow through the annulus section. The two pressure transducers and the temperature sensor, which are used to monitor the flow conditions, are mounted at the two ends of the test section.

Due to the limitation in the capability of the flow loop, only two flow regimes can be created, bubble flow and slug flow, which may not correspond the developed flow regime due to the limited flow rising length Nevertheless, the exact formation of flow regime is not the focus of this study, as previously mentioned that the main aim of this study is to present a monitoring method for rapidly imaging the prevailing flow regime in an annulus. Therefore, the experimental flow conditions were designed to cover these two flow regimes, along with the transitional flow regime from bubble flow to slug flow. The range of air flow rate used in the experiments was 10–60 SLPM (0.085–0.509 m/s superficial air velocity), while the range of water flow rate was 20–145 RPM (Rotation per Minute) (0.209–1.039 m/s superficial water velocity). The experimental flow conditions were split into three sets of conditions in terms of gas flow rate; Low gas flow rate (10–20 SLPM) to produce bubble flow regime, medium gas flow rate (30–50 SLPM) to produce bubble, slug and transitional flow regime, while high gas flow rate (60 SLPM) to give slug flow and transitional flow regime.

The ERT measurements, at each flow condition, were carried out, along with capturing photographs of the mixture flow through the cross-section of the annulus for latter evaluation of

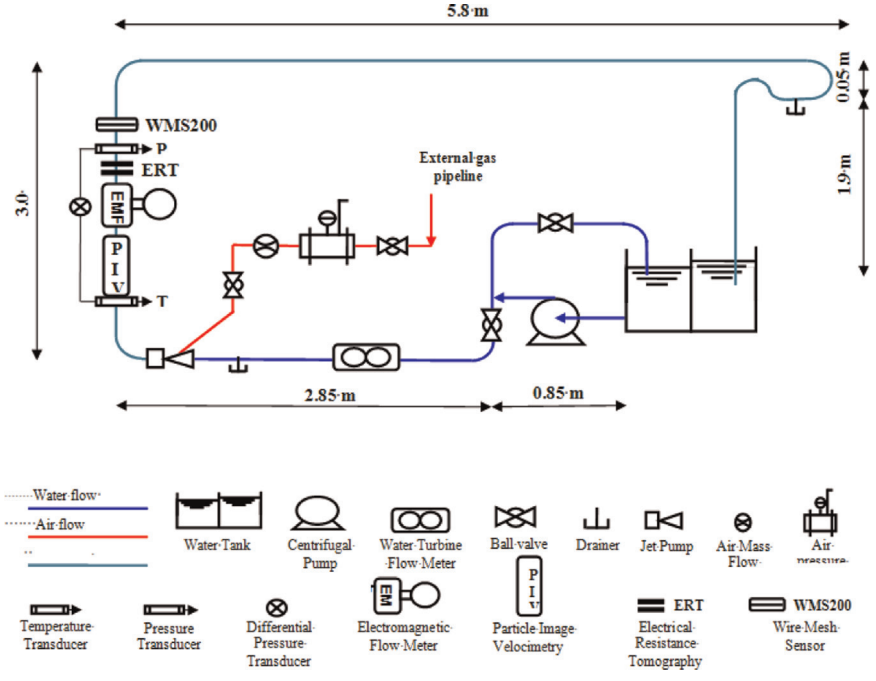

Fig. 4. The multiphase flow facility [10].

Please cite this article as: W. Na, et al., Imaging of gas–liquid annular flows for underbalanced drilling using electrical resistance tomography, Flow Measurement and Instrumentation (2015), http://dx.doi.org/10.1016/j.flowmeasinst.2015.07.003

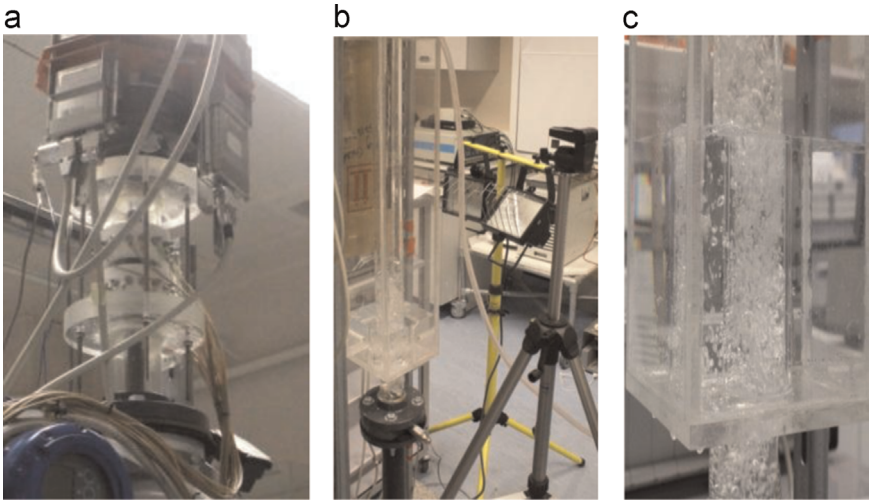

Fig. 5. Vertical test section, (a) dual-plane ERT sensor, (b) lighting facility and the observation section, and (c) cubical water filled observation section.

the ERT visualisation method. A high performance ERT measurement system (Fast Impedance Camera System-FICA or z8000) [22] was used to measure the flow of the mixture and capture the image of the cross-section of the annulus. The FICA system is an high performance ERT system, which is capable of acquiring 1000 dual frames per second. Each measurement data is averaged, through which the local air volume fraction profile is produced. The local air volume fraction is determined from the conductivity data using Maxwell relationship [11] formulated in Eq. (4). The ERT in principle measures the relative voltage difference between continuous flow (water) and mixture flow (air and water). This then used to calculate the local conductivity of each pixel located within the annulus region. The MSBP method described in Section 2.1 is used to convert the relative voltage difference to conductivity distribution (maps) of the cross-section of annulus under investigation. Based on the new sensitivity map generated in Section 2.1, the Sensitivity theorem based inverse solution using Conjugate Gradient (SCG) method [20] was used to reconstruct the off-line images of each flow condition. The reconstructed cross-sectional image shows annular area of air–water flow and solid steel rod.

4. Experimental results and discussion

All the ERT measurement data obtained from ERT (z8000 or FICA) system for each flow condition was collected and entered into P2000 software to produce the conductivity map and reconstructed image of the annular flow region. Each flow image was reconstructed using the SBP method with an improved sensitivity map, through which only the annular area was taken into account and the pixels, fall into the boundary of the inner pipe, are excluded. The conductivity map inverted was then imported into the software AIMFlow (Advanced Imaging and Measurement for Multiphase flow) to generate the tomograms of the annular region. The tomograms reconstructed for each flow condition were collected and analysed, so as to produce images of the annulus and to determine the local air volume fraction (void fraction). The cross-sectional image (or the tomogram) provides valuable information over the dynamic behaviour of each phase within the pipe and can readily be used for the purpose of visualisation. However, for detailed qualitative evaluation and visualisation, the air volume fraction profile may be more useful to visualise the internal structure of annular flow. Apart from the profiles, axial stacked images reconstructed using SCG were also produced, through which the dynamic of air and water can be visualised along the annulus section. 1000 frames (tomograms) generated by each plane were processed through an in house developed program to generate the stacked images. The program uses the selected nodes from each plane (mesh) and generates a text matrix, on which the final stacked images are based. The generated stacked images are illustrated below. In order to evaluate the visualisation scheme, the results obtained from the ERT are compared with visual observations (photograph), as discussed below.

For simplicity, only three conditions are selected and discussed in this paper. The selected conditions are bubble flow, which representative of low gas flow rate; transitional regime, which representative of medium gas flow rate and slug flow, which falls into the category of high gas flow rate. Figs. 6–8 show the test results, in which present (a) photographs; (b) stacked 1000 tomograms reconstructed with SCG algorithm (c) gas volume fraction profiles. Each stacked image has its individual colour range to visualise gas–liquid distribution.

Fig. 6 illustrates the concentric annuls bubble flow regime. The air flow rate used in this condition is 10 SLPM (0.085 m/s superficial velocity) and the water flow rate is 145 RPM (1.039 m/s superficial velocity). Fig. 6(a) shows the visual observation of the annulus. The stacked image of the mixture flow along the axial section of the annulus is shown in Fig. 6(b). The air volume fraction distribution (or concentration profile) across the cross-section of the annulus is illustrated in Fig. 6(c). The shaded area within the plots of each profile represents the inner pipe suspended concentrically in the outer pipe. Visual observation of the annulus region indicates a symmetrical distribution of air bubbles in the continuous phase across the cross-section of the annulus. However, it is quite apparent that the bubbles are relatively small and they are somehow in the form of discrete bubbles. The most pronounced phenomenon is that the bubbles are in a zig-zag fashion rising wrapped around the inner pipe rather than an equal radial distribution across the annulus. This phenomenon is well reflected in the air volume fraction profile obtained from the ERT. The highest air volume fraction (approximately 7.5%) can be seen close to the inner pipe wall, while the lowest air volume fraction (approximately 5%) can be observed close to the outer pipe wall. This may possibly be due to lift force action in small bubbles. The stacked images of air water flow along the annulus are illustrated in Fig. 6(b). The flow of each phase within the cross-section of the annulus is colour coded. The blue colour represents the dispersed phase (air), while the red colour represents the continuous phase (water). A section of the pipe is cut axially for better visualisation

Please cite this article as: W. Na, et al., Imaging of gas–liquid annular flows for underbalanced drilling using electrical resistance tomography, Flow Measurement and Instrumentation (2015), http://dx.doi.org/10.1016/j.flowmeasinst.2015.07.003

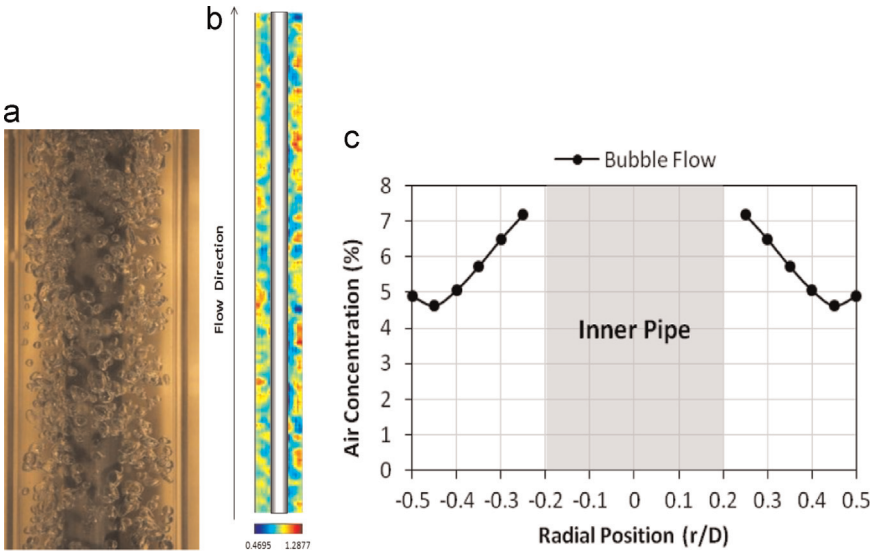

Fig. 6. Concentric annular bubble flow (*V*sa = 0.085 m/s, *V*sw = 1.039 m/s) (a) visual observation, (b) Stacked 1000 images of the mixture along axial section of the annulus, and (c) volume fraction profile. (For interpretation of the references to color in this figure, the reader is referred to the web version of this article.)

and evaluation of the image within the pipe. By observing the stacked images of air and water flow along the annulus, a symmetrical distribution of air and water can be seen across the cross-section of the annulus. It is also clear that the bubbles flow closer to the inner pipe wall, as it is suggested by the visual observation. It can also be seen that the profile slightly goes down close to the outer pipe wall, and then the peak takes on again. This could be attributed to the limitations associated with the sensitivity map, which is used for image reconstruction.

Fig. 7 shows the concentric annular transitional flow pattern from bubble flow to slug flow. Once the air flow rate increased from 10 SLPM (0.085 m/s air superficial velocity) to 30 SLPM (0.225 m/s air superficial velocity) and the water flow rate decreased from 145 RPM (1.039 m/s water superficial velocity) to 60 RPM (0.475 m/s water superficial velocity) it was noticed through visual observation that the flow of bubbles through the cross-section of the annulus had almost similar characteristics to those flow in a circular full bore pipe. With the increase of air flow rate the number of bubbles increase and move as packed bubbles. This leads to the increase of air density within the annulus region. With the increase of density it is apparent that the bubbles flow faster in upward vertical section in a zig-zag fashion but interleaved with large bubbles. The higher number of bubbles in the flowing media and their faster movement increases the rate of collision and rate of agglomeration among the packed bubbles. As a result, larger bubbles are formed occasionally, which eventually leads to slug flow if the air flow rate is further increased. This phenomenon can be noticed in the visual observation in Fig. 7(a). Similar to bubble low, the highest air volume fraction can be seen close to the inner pipe wall. The movement and distribution of each phase, air and water, is clearly highlighted in the stacked images shown in Fig. 7(b). By comparing the staked images with the visual observation, a reasonably accurate representation of flow shown in the visual observation can be noticed. With regard to the gas volume fraction profile, it is apparent that highest air volume fraction is again present close to the inner pipe wall, which well agrees with the visual observation (photograph).

In slug flow, as it is shown in Fig. 8, the air flow rate is 50 SLPM (0.425 m/s air superficial velocity) and water flow rate is 40 RPM (0.342 m/s water superficial velocity). Similar trend can be

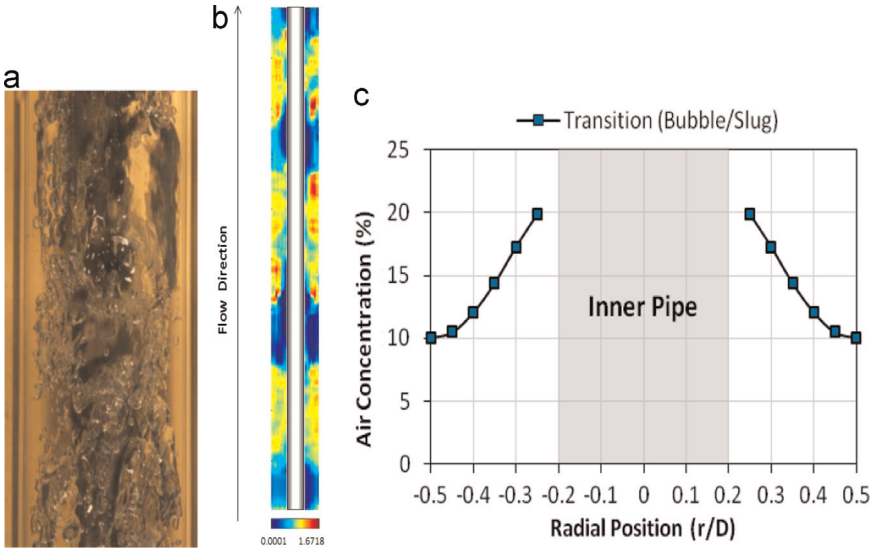

Fig. 7. Concentric annular transitional from bubble to slug (*V*sa = 0.225 m/s, *V*sw = 0.475 m/s) (a) visual observation, (b) stacked 1000 images of the mixture along axial section of the annulus, and (c) volume fraction profile.

Please cite this article as: W. Na, et al., Imaging of gas–liquid annular flows for underbalanced drilling using electrical resistance tomography, Flow Measurement and Instrumentation (2015), http://dx.doi.org/10.1016/j.flowmeasinst.2015.07.003

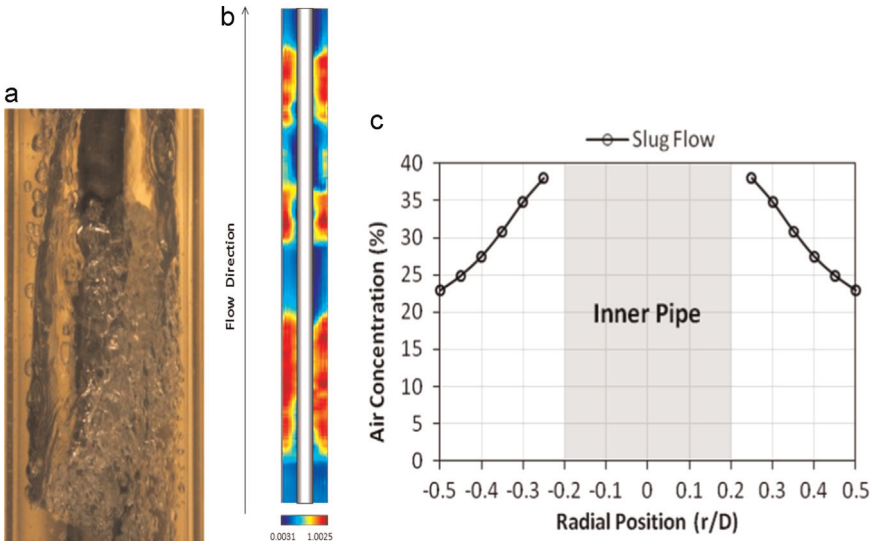

Fig. 8. Concentric annular slug flow (Vsa = 0.425 m/s, Vsw = 0.342 m/s) (a) visual observation, (b) Stacked 1000 images of the mixture flow along axial section of the annulus, and (c) volume fraction profile.

Table 1
Mean air volume fraction across the cross-section of the annulus.

Mean air volume fraction	Bubble	Transitional (bubble–slug)	Slug
ERT	0.06	0.14	0.3
Inlet	0.07	0.36	0.58

observed as that of bubble flow and transitional flow regime. The air phase has a tendency of flowing closer to the inner pipe wall, similar to that of bubble and transitional regime. The range of air volume fraction within the annulus is shown by the volume fraction profile as approximately 23–37%. The highest air volume fraction can be seen close to the inner pipe wall in both, the visual observation and air volume fraction profile. This phenomenon is also suggested by the stacked images of the flowing mixture within the pipe annulus, shown in Fig. 8(b). It can be seen that the air flows as large bubbles. The shape of large bubbles present in the annulus region is noticeably different to that flowing in a circular full bore pipe. The shape of larger bubbles flowing through the annulus is somehow elongated and moving in an asymmetrical fashion. Some dispersed bubbles can also be seen, which are carried by the liquid in the area close to the outer pipe wall. These dispersed bubbles are formed as a result of collision of water with larger bubbles as the water falls downward into the region that is not occupied by the larger bubbles.

The mean air volume fraction obtained from ERT across the cross-section of the annulus, and mean air volume fraction based on inlet flow conditions are shown in Table 1. It is worth pointing out that the inlet air volume fraction is determined based on standard conditions (1.01 bar and 21.1 °C). It is quite apparent that the air volume fractions at standard conditions can be converted to actual volume fraction (at loop temperature and pressure) for the purpose of comparison and evaluation of the measured values. However, as the main focus of this work is merely on flow visualisation rather than flow metering, the evaluation of measured air volume fraction is beyond the scope of this paper. Therefore, the results highlighted in Table 1, are only an indication of ERT measured mean air volume fractions against their respective inlet volume fractions.

5. Conclusions

A high performance ERT technique is proposed for visualisation of two-phase gas–liquid flow in an annulus with a metallic inner pipe. The ERT using a revised sensitivity map and a mesh file with corresponding boundary conditions is used to interrogate the internal structure of annular flow for bubble, transitional and slug flows. Axial flow regimes are compared with visual observations. Although tomographic images cannot be as clear as the photographs captured during the measurements, ERT is still able to provide enough information regarding the prevailing flow regime within the annulus. The air volume fraction profiles in the annulus region, produced from the ERT, indicate a good agreement between the profiles and visual observation (photographs). The stacked images are reasonably accurate representation of air water in the annulus region for the conditions used in this study. Further work will be carried out to evaluate gas flow profiles with other references.

Acknowledgement

The research was supported by the Open Fund of State Key Laboratory of Oil and Gas Geology and Exploration at Southwest Petroleum University (PLN1119), National Natural Science Foundation of China (51204140, L1322021 and 51334003). Authors would like to thank Mr. Yunjie Yang for preparing the figures of the sensitivity matrix.

References

[1] D.C. Barber, B. Brown, Applied potential tomography, J. Phys. E: Sci. Instrum. 17 (1984) 723–733.
[2] Bourgoyne Jr., T. Adam, Rotating control head applications increasing, Oil Gas J. (1995) 72.
[3] S. Ghosh, D.K. Pratihar, B. Maiti, P.K. Das, Automatic classification of vertical counter-current two-phase flow by capturing hydrodynamic characteristics through objective descriptions, Int. J. Multiph. Flow 52 (2013) 102–120.
[4] C. Olerni, J. Jia, M. Wang, Measurement of air distribution and void fraction of an upwards air–water flow using electrical resistance tomography and a wire-mesh sensor, Meas. Sci. Technol. 24 (3) (2013) 1–9.
[5] P.J. Holden, M. Wang, R. Mann, F.J. Dickin, R.B. Edwards, Imaging stirred-vessel macromixing using electrical resistance tomography, Am. Inst. Chem. Eng. J. 44 (4) (1998) 780–790.
[6] J. Jia, M. Wang, Y. Faraj, Evaluation of EIT systems and algorithms for handling

full void fraction range in two-phase flow measurement, Meas. Sci. Technol. 26 (1) (2015).
[7] E. Julia, T. Hibiki, Flow regime transition criteria for two-phase flow in a vertical annulus, International Journal of Heat and Fluid Flow 32 (2011) 993–1004.
[8] Kjell, K.F., Rommetveit, R., Merlo, A., 2003. Improvements in dynamic modeling of underbalanced drilling. In: Proceedings of the IADC/SPC Underbalanced Technology Conference and Exhibition, SPE-81636-MS, 25–26 March.
[9] C.J. Kotre, EIT image reconstruction using sensitivity weighted filtered backprojection, Physiol. Meas. 15 (Suppl. 2A) (1992) S125–S136.
[10] H. Li, M. Wang, Y. Wu, G. Lucas, Volume flow rate measurement in vertical oil-in-water pipe flow using electrical impedance tomography and a local probe, Multiph. Sci. Technol. 21 (2009) 81–93.
[11] J.C.A. Maxwell, Treatise on Electricity and Magnetism, (Unabridged) 3rd edition, Dover Publications Inc., New York, 1873.
[12] W. Na, Y.F. Meng, Cuttings transport models and experimental visualization of underbalanced horizontal drilling, Math. Probl. Eng. Vol. 2013 (2013) ID764782.
[13] U. Puli, A.K. Rajvanshi, P.K. Das, Investigation of bubble behavior in subcooled flow boiling of water in a horizontal annulus using high-speed flow visualization, Heat Transf. Eng. 34 (10) (2012) 838–851.
[14] D. Reitsma, R.E. Van, Utilizing an automated annular pressure control system for managed pressure drilling in mature offshore oilfields, J. SPE (2005) 96646.
[15] Shale, L.T., 1994. Underbalanced drilling: formation damage control during high-angle or horizontal drilling. Paper SPE 27351 Presented at the International Symposium of Formation Damage Control held in Lafayette, LA, February 7–10 1994.
[16] M. Sharifi, B. Young, Electrical resistance tomography (ERT) applications to chemical engineering, Chem. Eng. Res. Des. 91 (9) (2013) 1625–1645.
[17] C. Tan, S.J. Ren, F. Dong, Reconstructing the phase distribution within an annular channel by electrical resistance tomography, Heat Transf. Eng. 36 (12) (2015) 1053–1064.
[18] Taylor, J., McDonald, C., Fried, S., 1995. Underbalanced drilling total system approach. Presented at the 1st International Underbalanced Drilling Conference and Exhibition, The Hague, Netherlands, October 2–4 1995.
[19] Wang, M., Mann, R., Dickin, F.J., 1996. A Large scale tomographic sensing system for mixing processes, In: Proceedings of the IWISP'96 (for 3rd International Workshop on Image and Signal Processing Advances in Computational Intelligence in Manchester), Elsevier Science B.V., pp. 647–650.
[20] M. Wang, Inverse solutions for electrical impedance tomography based on conjugate gradients methods, Meas. Sci. Technol. IOP 13 (2002) 101–117.
[21] M. Wang, T.F. Jones, R.A. Williams, Visualisation of asymmetric solids distribution in horizontal swirling flows using electrical resistance tomography. Part A, Trans IChemE 81 (2003) 854–861.
[22] M. Wang, Y. Ma, N. Holliday, Y. Dai, R.A. Williams, G. Lucas, A High-performance EIT System, IEEE Sens. J. 5 (2) (2005) 289–299.
[23] M. Wang, R. Mann, F.J. Dickin, Electrical resistance tomographic sensing systems for industrial applications, Chem. Eng. Commun., 175, (1999) 49–70.
[24] R.A. Williams, X. Jia, R.M. West, M. Wang, J.C. Cullivan, J. Bond, I. Faulks, T. Dyakowski, S.J. Wang, N. Climpson, J.A. Kostuch, D. Payton, Industrial monitoring of hydrocyclone operation using electrical resistance tomography, Miner. Eng. 12 (10) (1999) 1245–1252.

Please cite this article as: W. Na, et al., Imaging of gas–liquid annular flows for underbalanced drilling using electrical resistance tomography, Flow Measurement and Instrumentation (2015), http://dx.doi.org/10.1016/j.flowmeasinst.2015.07.003